Effect of micro-arc oxidation surface modification of 3D-printed porous titanium alloys on biological properties

Renhua Ni[1,2#], Zehao Jing[1,2,3#], Chenao Xiong[1,2], Dexuan Meng[1,2], Chongbin Wei[4], Hong Cai[1,2]

[1]Department of Orthopedics, Peking University Third Hospital, Beijing, China; [2]Engineering Research Center of Bone and Joint Precision Medicine, Ministry of Education, Beijing, China; [3]Beijing Key Laboratory of Spinal Disease Research, Beijing, China; [4]Beijing AK Medical Co., Ltd., Beijing, China

Contributions: (I) Conception and design: R Ni, Z Jing; (II) Administrative support: H Cai; (III) Provision of study materials or patients: C Wei; (IV) Collection and assembly of data: R Ni, C Xiong, D Meng; (V) Data analysis and interpretation: R Ni, Z Jing; (VI) Manuscript writing: All authors; (VII) Final approval of manuscript: All authors.

[#]These authors contributed equally to this work.

Correspondence to: Hong Cai. Department of Orthopedics, Peking University Third Hospital, Beijing 100191, China. Email: hongcai@bjmu.edu.cn; Chongbin Wei. Beijing AK Medical Co., Ltd., Beijing 102200, China. Email: chongbin.wei@ak-medical.net.

Background: Three-dimensional (3D) printing technology has been widely used in orthopedics; however, it is still limited to the change of macroscopic structures. In order to further improve the biological properties of 3D-printed porous titanium scaffolds, this study introduced micro-arc oxidation (MAO) technology to modify the surface of porous titanium scaffolds and construct bioactive coatings on the surface of porous titanium scaffolds to improve the biocompatibility and osseointegration ability of the material.

Methods: For *in vitro* experiments, human bone marrow stem cells (hBMSCs) were seeded onto untreated scaffolds (control group) and MAO-treated scaffolds (experimental group). After 24 h of co-culture, cytotoxicity was observed using live/dead staining, and cell/scaffold constructs were retrieved and processed for the assessment of cell morphology by using scanning electron microscopy (SEM). Cell proliferation was detected using the Cell Counting Kit-8 (CCK-8) assay after 3, 7, and 14 days of co-culture. The levels of alkaline phosphatase (ALP) in the cell supernatant were detected after 7 and 14 days of co-culture. For *in vivo* experiments, micro-computed tomography (micro-CT) and Masson Goldner's staining were used to evaluate bone ingrowth and osseointegration at 4 and 8 weeks postoperatively.

Results: *In vitro* experiment results confirmed that the two groups of scaffolds were non-cytotoxic and the cell adhesion status on the MAO-treated scaffolds was better. Over time, cell proliferation and ALP levels were higher in the MAO-treated group than in the untreated scaffolds. In the *in vivo* experiments, the MAO-treated scaffolds showed better bone ingrowth and osseointegration than the untreated group at different time points.

Conclusions: The MAO-treated porous titanium scaffold formed a uniform and dense bioactive coating on the surface, which was more conducive to cell adhesion, proliferation, and differentiation and showed better osseointegration and bone ingrowth *in vivo*.

Keywords: Three-dimensional printing (3D printing); micro-arc oxidation (MAO); biocompatibility; osseointegration

Introduction

Loosening of the bone-implant interface is one of the main causes of implant failure (1). Common materials used for orthopedic implants can be broadly classified into three categories: metals, ceramics, and polymers (2). Metal implant prostheses are still the preferred choice for orthopedic surgery, despite the proliferation of new biomaterials (3). Titanium and its alloys have become the main materials used in metal implant prostheses because of their low density, low toxicity, structural stability, superior mechanical properties, and biocompatibility (4). However, in contemporary clinical applications, the integration between the implant prosthesis and the bone tissue interface is affected by the traditional machined titanium implants because of their weak osteogenic induction capacity and high elastic modulus, which leads to a significant stress-masking effect (5,6).

Advances in science and technology have led to the initial use of three-dimensional (3D) printing technology in the design and preparation of orthopedic implant prostheses. Computer-assisted design (CAD) software is used to design a 3D bone trabecular structure similar to real bone tissue that can accurately simulate the porous structure of human cancellous bone. This can effectively reduce the elastic modulus of the implant prosthesis and reduce the stress-masking effect, thus achieving the goal of promoting bone tissue growth, reducing bone tissue dissolution and resorption, and helping better integrate the bone tissue interface with the implant prosthesis (7,8). The complex and interconnected pore structures constructed using 3D printing technology can help ingrowth of bone and blood vessels (9-11). However, changing the macro structure of 3D-printed porous scaffolds simply cannot promote the proliferation and differentiation of osteoblasts, and filament diameter less than 100 μm can affect the mechanical properties of scaffolds (12).

Experiments have been carried out using 3D-printed titanium scaffolds in sheep and the results were found to be unsatisfactory in terms of bone ingrowth at 12 weeks (13). Studies have shown that the changing surface morphology and preparing bioactive coatings of the material can significantly impact the biocompatibility of 3D-printed porous titanium alloys (14,15). Therefore, it is crucial to modify the coated surface of 3D-printed porous titanium alloy scaffolds.

Micro-arc oxidation (MAO), also known as anodic plasma chemical oxidation, is a special electrochemical surface treatment technique. Typical valve metals (e.g., titanium, aluminium, and magnesium) are used as anodes and a certain voltage is applied over a certain range to produce an electrical discharge on the metal surface and an oxide coating with a microporous structure (16). Changes in the voltage, current, electrolyte composition, and process duration can influence the quality of the coatings (17). It has been confirmed that the oxide coating formed on the surface of the titanium alloy via MAO can effectively reduce the content of Al and V so that the biocompatibility of the material is improved (18). In addition, a study showed that the fabrication of bioactive Ca/P coating on the magnesium alloy surface via MAO can improve the regeneration of bone tissue (19).

MAO enables simultaneous chemical and morphological modification of the implant surface through a single process (20). This technique is mainly performed in solution and is therefore suitable for the surface treatment of complex porous geometries, achieving homogeneous surface modification inside and outside the porous titanium alloy support and *in situ* generation of oxide ceramic films (21-23). However, it is difficult to modify the cavity surface of porous materials by line of sight machining techniques (24).

In this study, we constructed a micro-nanoscale bioactive coating on the surface of an electron beam melting (EBM)-manufactured porous Ti₆Al₄V scaffold through MAO treatment. The biocompatibility and osteogenic differentiation ability of the treated scaffolds were verified using *in vitro* cell experiments. The osseointegration and bone ingrowth capacity of the treated scaffolds was preliminarily investigated using a rabbit bone defect model. This study aimed to evaluate the efficacy of MAO treatment towards improving the *in vitro* and *in vivo* bioactivity of 3D-printed porous Ti₆Al₄V scaffolds for bone defect reconstruction. We present the following article in accordance with the ARRIVE reporting checklist (available at https://atm.amegroups.com/article/view/10.21037/atm-22-2536/rc).

Methods

Sample fabrication

All samples were prepared using an EBM S12 system (Arcam AB, Sweden). The porous structure was designed based on a bionic trabecular structure unit cell using CAD software (10). The porous Ti₆Al₄V scaffold was printed with a pore size of 640 μm, filament diameter of 400 μm, and

porosity of 73%, as previously described (25).

Sample specifications were as follows: (I) diameter =5 mm, cylinder with height =6 mm suitable for material characterization experiments (except contact angle tests) and animal experiments; (II) diameter =8 mm, cylinder with height =5 mm suitable for *in vitro* cell experiments; (III) titanium alloy discs with diameter =10 mm and height =1 mm were prepared for the contact angle tests to reduce the influence of the macroscopic porous structure on the measurement angle.

Surface treatment

All samples were ultrasonically cleaned in acetone, alcohol, and distilled water, and dried at 60 ℃ overnight. Subsequently, porous Ti_6Al_4V scaffolds were used as the anode, and a stainless plate was used as the cathode in an electrolytic bath. The electrolyte was prepared by dissolving 0.065 M $Ca(CH_3COO)_2·H_2O$, 0.03 M NaH_2PO_4, 0.065 M EDTA-2Na, and 0.5 M NaOH in deionised water and then treated at a working voltage of 350 V, pulse frequency of 500 Hz, and duty ratio of 10% for 5 min. The bath temperature was maintained below 40 ℃ using water for cooling.

Surface characterizations

The surface views of the samples were observed by scanning electron microscopy (SEM; S-4800, Hitachi), and energy-dispersive X-ray spectroscopy (EDS) was used to evaluate the elemental composition of the sample surfaces. X-ray photoelectron spectroscopy (XPS; Kratos, UK) was used to analyze the chemical compositions of the samples that were treated using the same MAO treatment. The crystallinity of the coating was investigated using an X-ray diffractometer (XRD; D8 Focus, Bruker) equipped with a Cu-Kα source (λ=1.54 Å) at 40 kV and 50 mA in the range of 2θ=10°–80°. Hydrophilicity was tested using a contact angle measuring instrument (Kino, USA).

In vitro cell experiments

Primary human bone marrow stem cells (hBMSCs; passage 3, Lonza, USA) were cultured with an atmosphere of 5% CO_2 at 37 ℃. Scaffolds wetted with minimum essential media (MEM) medium (Lonza, USA) were placed in 48-well plates and $2×10^4$ cells per mL suspension were drop-seeded onto the untreated and MAO-treated scaffolds.

Cytotoxicity

The cells were co-cultured with the prepared samples for 24 h, added to the configured live/dead working solution, incubated for 30 min at 37 ℃, protected from light, and observed under a laser confocal microscope (Leica, Japan).

Cell adhesion

After 24 h of incubation, cells were fixed in 2.5% glutaraldehyde at 25 ℃ for 1 h. After gradient ethanol dehydration and critical point drying with a gold spray, SEM was used to observe the adhesion status of the cells.

Cell proliferation

After 3, 7, and 14 days of incubation, cell proliferation was assessed using the Cell Counting Kit-8 (CCK-8; Dojindo, Japan). At each time point, 1:10 CCK-8 diluted solution was added and incubated for 3 h at 37 ℃, protected from light. Absorbance was measured at a wavelength of 450 nm.

Cell differentiation

Osteoblast differentiation ability was assessed *in vitro* by testing the alkaline phosphatase (ALP) activity of hBMSCs. The cells were seeded on the samples for 24 h, and then the medium was changed. Osteogenic medium (Lonza, USA) for inducing osteogenic differentiation contained 0.5% ascorbate, 0.5% dexamethasone, and 1% β-glycerophosphate. After 7 and 14 days of osteogenic induction on the scaffold, 500 µL lysate was added to the 48-well plates with the samples, and the cells were sonicated. Then, the lysate was centrifuged at 12,000 r/min for 5 min at 4 ℃. Absorbance values were measured at 405 nm using the ALP assay kit (Beyotime, China) and at 562 nm using the BCA protein assay kit (Beyotime, China). The ratio of the absorbance at 405 nm to that at 562 nm was used as the quantitative value of ALP.

Animal experiments

Experiments were performed under a project license (No. LA2014214) granted by Experimental Animal Ethics Committee of Peking University, in compliance with national guidelines for the care and use of animals. A protocol was prepared before the study without registration. Before the experiment, all experimental animals were reared in a solitary cage for 1 week before surgery to adapt to the environment. Environmental interference was eliminated, the diet was standardized, and ethical principles were followed. Eight mature male New Zealand rabbits

Page 4 of 11

Ni et al. MAO modification of porous Ti$_6$Al$_4$V

weighing an average of 3,500 g were used in each group for the experiments. The surgery was performed under standard sterile conditions. After anesthesia via an injection of amiodarone (50 mg/kg), the lateral condyle of the femur was carefully exposed through a skin incision and muscle blunt dissection. A bone defect of 5 mm in diameter and 6 mm in depth was constructed in the lateral femoral condyle of the rabbit and two groups of scaffolds were implanted. At 4 and 8 weeks postoperatively, the femur of the rabbit was removed.

Micro-computed tomography (micro-CT) analysis

Sixteen specimens (including 8 left and 8 right femur specimens) from each group were scanned by micro-CT (Siemens, Munich, Germany) using an Inveon Acquisition Workplace (Siemens, Munich, Germany) at a resolution of 9 μm, current of 80 mA, voltage of 80 kV, and 2,500 ms exposure time in each of the 360 rotational steps. The micro-CT images were then reconstructed using multimodal 3D visualization software (Inveon Research Workplace, Siemens, Munich, Germany). After reconstruction, the peripheral 600 μm around and the intra-porous space within the implant were selected as the regions of interest (ROIs). In the ROI, the bone volume/tissue volume (BV/TV; the ratio of bone volume to total volume) and trabecular separation (Tb. Sp; mean width of the medullary cavity between bone trabeculae) were automatically calculated.

Histological evaluation

After being scanned by micro-CT, 16 femur specimens from each group were fixed in 10% formalin for 14 days and dehydrated in gradient ethanol solution (40%, 75%, 95%, and 100%) for 3 days each. Then, the specimens were embedded in methyl methacrylate. The EXAKT system (EXAKT Apparatebau, Norderstedt, Germany) was used to cut the embedded samples into 200 μm thick sections. Sandpapers were used to ground these sections to a thickness of 40–50 μm. These final sections were subjected to Masson Goldner's trichrome staining. The stained sections were observed under an optical microscope (BH-2; Olympus America Inc., USA).

Statistical analysis

For all experiments, data are reported as mean ± standard deviation (SD). Statistical analysis was performed using one-way analysis of variance (ANOVA) combined with the Student-Newman-Keuls (SNK) post hoc test in SPSS 24.0. Significance and high significance were defined as P values of less than 0.05 and 0.01, respectively.

Results

Characterizations of the coatings

SEM images showed a large number of crater-like micro-nano porous structures with various pore sizes on the surface of the MAO-treated scaffolds, whereas the untreated scaffolds had smoother surfaces. The MAO-treated scaffold sections had coatings with a thickness of 1–2 μm, which only slightly influenced the macrostructure of the scaffold (*Figure 1*). As revealed by EDS analysis (*Figure 2*), the coatings contained a high Ca/P ratio on the scaffold surface (approximately 1.84), which was close to that observed in the mineral phase of the bone (the Ca/P ratio of hydroxyapatite is approximately 1.67). A study showed that a high Ca/P ratio scaffold promoted osteoclast production and TGF-β1 secretion, thereby significantly promoting bone healing (26). It is hypothesized that the MAO-treated porous titanium scaffold with a high Ca/P ratio has an increased bone healing capacity.

The XPS results suggested that the main elements of the coating were O, Ti, Ca, C, and P. The core layer spectral doublet of Ti2p was formed by the spin-orbit splitting of Ti2p3 (458.5 eV) and Ti2p1 (454 eV) in TiO$_2$. The core layer spectrum of Ca2pd was dominated by Ca2p1 and Ca2p3 with binding energies at 345 and 347.5 eV, respectively, corresponding to Ca^{2+} for the different inorganic calcium oxide compounds. In the O1s high-resolution mapping, 3 peaks were observed at 529, 532, and 533 eV, corresponding to the chemical bonds Ti-O-Ti, Ti=O (or H$_2$O), P=O- bond, respectively. In the P2P profile, the binding energies of the multiple peaks associated with P^{5+} are shown as P$_2$O$_7^{4-}$ (134.5 eV), HPO^{4-} (133.5 eV), and PO$_4^{3-}$ (132.6 eV). These results suggest that the dominant coating compounds are titanium dioxide and apatite, which comprise a mixture of hydrated Ca$_2$P$_2$O$_7$, CaHPO$_4$, and Ca$_3$(PO$_4$)$_2$ (*Figure 3*).

XRD analysis was performed to determine the phase states of the coating components. For the MAO-treated scaffold, apart from the diffraction peaks arising from the Ti$_6$Al$_4$V substrate, relatively sharp peaks corresponding to well-crystallized anatase and rutile were clearly present on the surface (*Figure 3*).

To reduce the influence of macroscopic porosity on
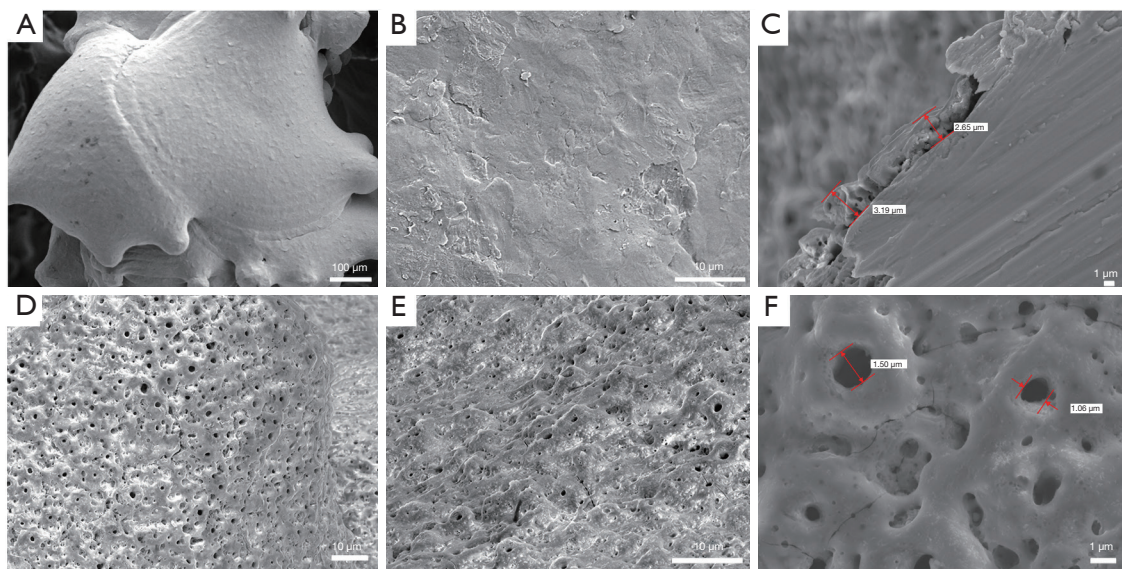
Figure 1 Representative SEM images of the untreated and MAO-treated Ti_6Al_4V scaffolds. (A,B) Smooth surface of the untreated scaffold. (D,E) Microporous structure of the surface of the MAO-treated scaffold. (C,F) Thickness of the coating and pore sizes. SEM, scanning electron microscopy; MAO, micro-arc oxidation.

Figure 2 Representative EDS analysis of the MAO-treated Ti_6Al_4V scaffold. EDS, energy-dispersive X-ray spectroscopy; MAO, micro-arc oxidation.

contact angle measurements, a titanium alloy disc was used for this test. Sample number in each group is 4. The contact angle results for the MAO-treated and untreated samples were 21.035°±0.386° and 99.682°±2.764°, respectively (n=4) (*Figure 4*). A previous study showed that cells adhered and proliferated better on the surface of a more hydrophilic material (27). Based on the test results, it can be inferred that the MAO-treated scaffold had better biocompatibility.

In vitro results

Cell adhesion
After co-culture for 24 h, cell adhesion morphology of

the scaffolds in the two groups was observed using SEM. Compared to the untreated group, the hBMSCs in the MAO-treated group spread into polygonal or elongated shapes with obvious microfilament and pseudopod structures and more spreading morphology, and the cells exhibited more pseudopods anchored into the micropores and adhered more firmly to the material (*Figure 5*).

Biocompatibility and ALP activity
In the live/dead staining experiment, the cells survived on all scaffolds, as observed by their staining patterns on the scaffolds where no staining of dead cells (red staining) could be visualized. After co-culture for 24 h, the cells that

Page 6 of 11

Ni et al. MAO modification of porous Ti$_6$Al$_4$V
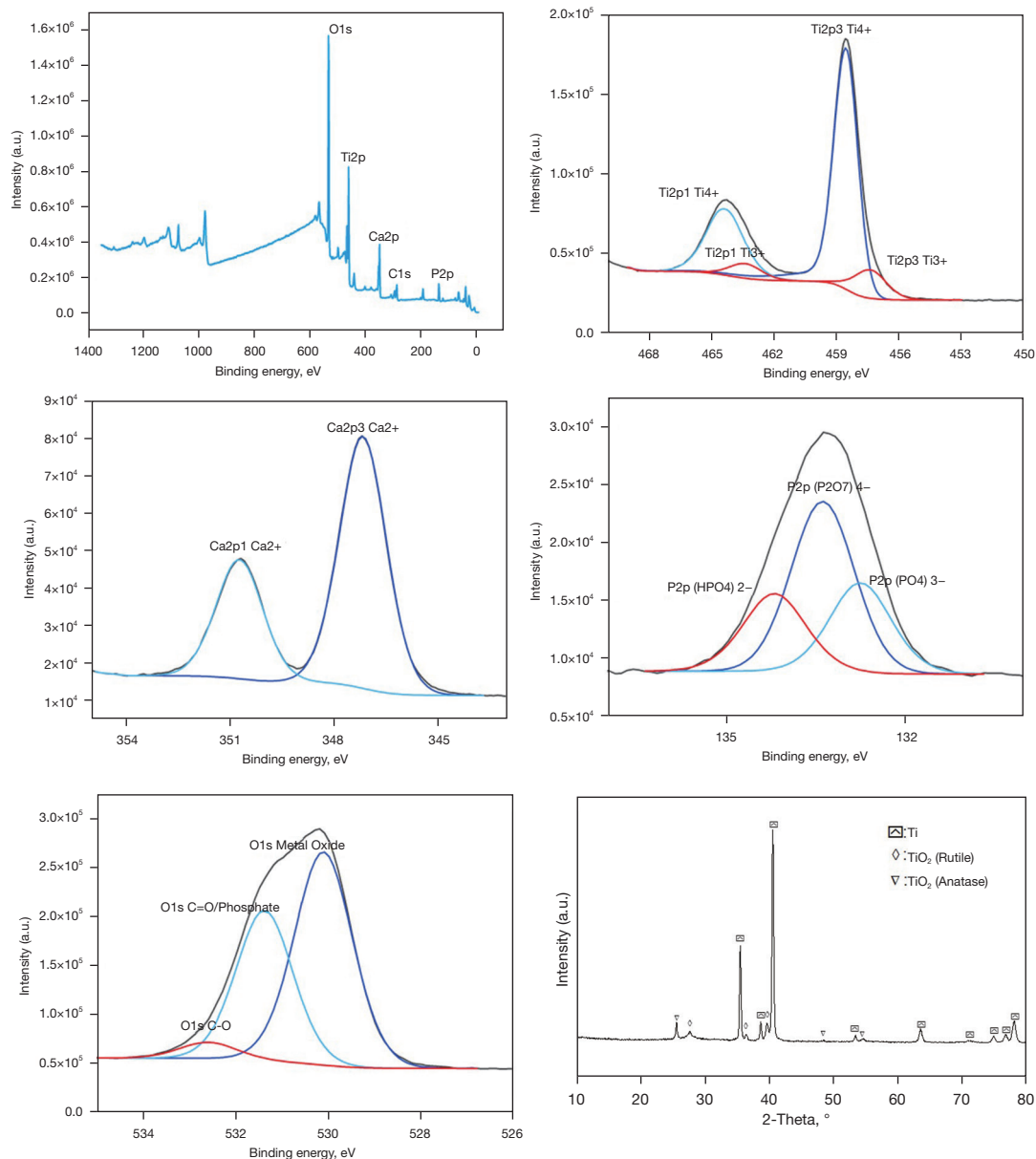
Figure 3 XPS and XRD patterns for the MAO-treated scaffold. XPS, X-ray photoelectron spectroscopy; XRD, X-ray diffractometer; MAO, micro-arc oxidation.

survived on the scaffolds were observed as a clear green color. Both groups showed no obvious red fluorescence. This indicated that there was no obvious cytotoxicity in either scaffold group. Owing to the irregularity of the macroscopic porous structure, an uneven distribution of cells was observed (*Figure 6A*).

The cellular metabolic activity at different time points reflected the cell proliferation of hBMSCs on the two groups of scaffolds. In general, the MAO-treated group

exhibited a higher level of cell proliferation than the untreated group (*Figure 6B*). ALP is an early marker of cellular osteogenesis. To compare the osteoblastic differentiation of hBMSCs on the two groups of scaffolds, the quantitative ALP assay was performed. The ALP activity of the treated group was significantly higher than that of the control group after 7 days of co-culture. After co-culture for 14 days, the statistical results of the MAO-treated group differed even more significantly from those of
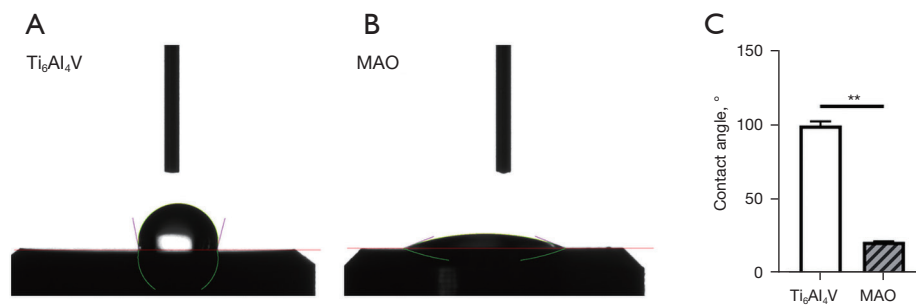
Figure 4 Hydrophilic testing of untreated Ti_6Al_4V and MAO-treated Ti_6Al_4V. (A,B) Representative images of the contact angle test. (C) Statistical analysis of the contact angle of the two types of scaffolds. **, P<0.01. Sample number in each group is 4. MAO, micro-arc oxidation.
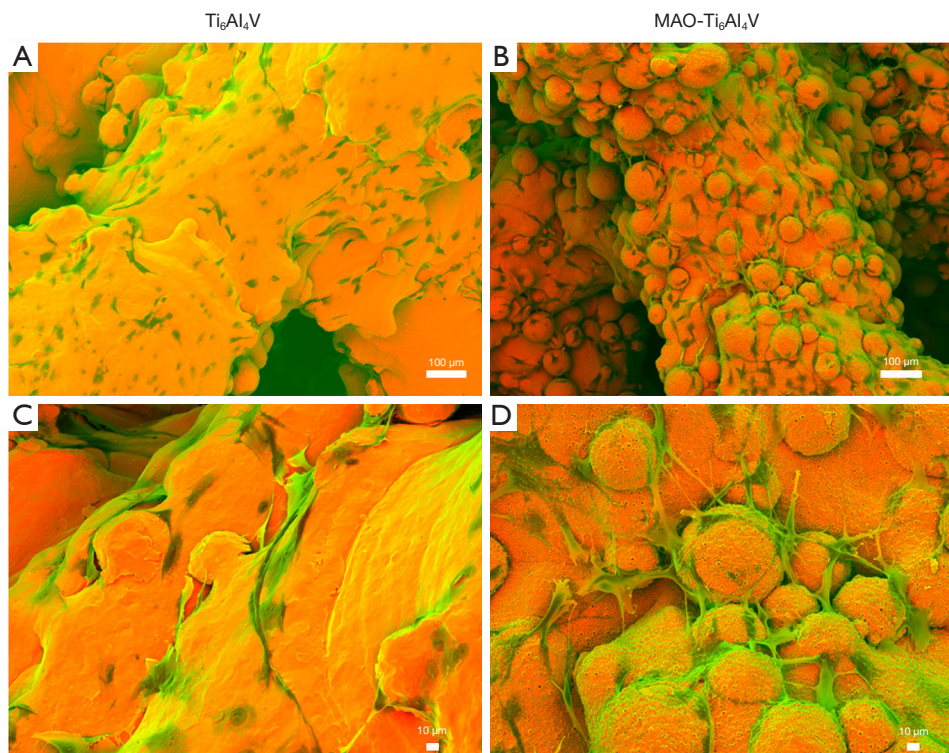
Figure 5 SEM observation after 24 h of cell culture. (A,C) Cells adhered to Ti_6Al_4V scaffold at different magnifications. (B,D) Cells adhered to MAO-treated Ti_6Al_4V scaffold at different magnifications. MAO, micro-arc oxidation; SEM, scanning electron microscopy.

the untreated group (*Figure 6C*).

In vivo results

Micro-CT analysis

Osteogenesis was quantified using micro-CT. Two indicators, namely BV/TV, positively associated with osteogenesis, and Tb. Sp, negatively associated with osteogenesis, were calculated.

As illustrated in *Figure 7A,7B*, BV/TV increased over time while Tb. Sp decreased, indicating that more osteogenesis occurred. The MAO-treated group showed significantly higher bone formation in this region than the untreated group (P<0.05).

Page 8 of 11

Ni et al. MAO modification of porous Ti$_6$Al$_4$V
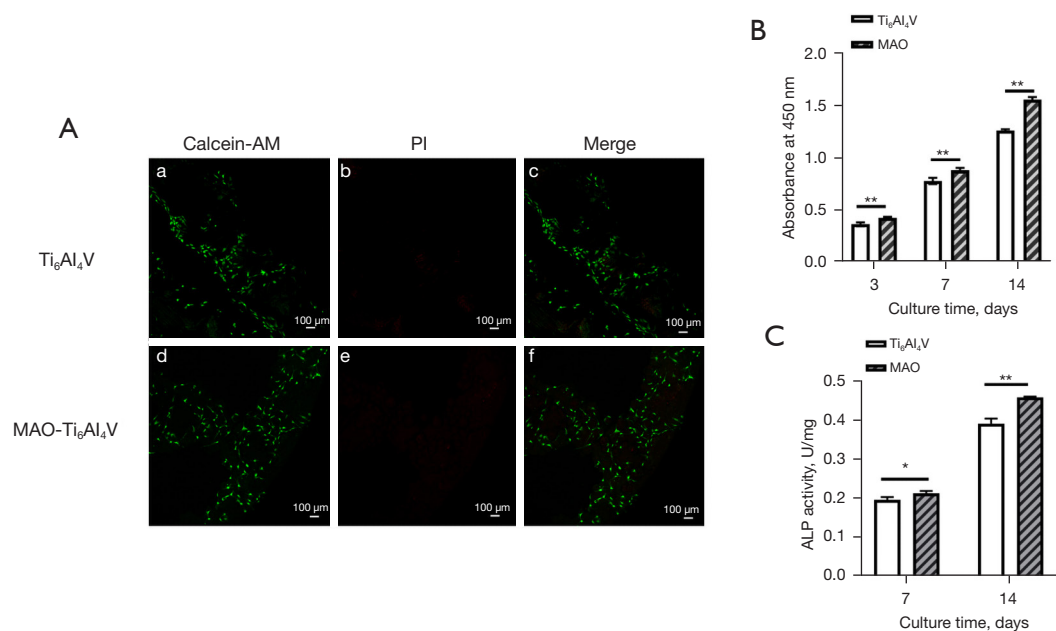
Figure 6 Biocompatibility and osteogenic differentiation of hBMSCs on two groups of scaffolds. (A) Live/dead staining of the scaffolds after 24 h of cell culture. Calcein-AM solution stained live cells and PI solution stained dead cells. Staining plots of live cells on the untreated scaffold and MAO-treated scaffold, respectively (a,d). Staining plots of dead cells on the untreated scaffold and MAO-treated scaffold, respectively (b,e). Mixed plots of live and dead cells on the untreated scaffold and MAO-treated scaffold (c,f). There were no obvious dead cells (red staining) on either type of scaffolds. (B) Cell proliferation on the untreated and MAO-treated scaffolds. (C) ALP activity of the untreated and MAO-treated scaffolds after 7 and 14 days of cell culture. *, $P<0.05$; **, $P<0.01$. MAO, micro-arc oxidation; PI, propidium iodide; ALP, alkaline phosphatase; hBMSCs, human bone marrow stem cells.

Qualitative histological results

Bone ingrowth and osseointegration were evaluated via undecalcified histology. The specimens were subjected to Masson Goldner's trichrome staining to distinguish mineralized bone tissues. Observed under the optical microscope, the bone tissues appeared in green/blue, osteoid tissues appeared in red/orange, and the scaffolds appeared in black.

Figure 7C shows representative light optical micrographs of the cross-sectioned scaffolds in the femoral condyle at 4 and 8 weeks. At 4 weeks, the untreated group only had osteoid tissue formation around the scaffold, whereas the MAO-treated group had more osteoid tissues around and inside the scaffold. Both groups had less mineralized bone. At 8 weeks, the osteoid tissues in both groups gradually mineralized. Bone tissue surrounding each microfilament was observed. The bone tissue generated in the MAO-treated group was in close contact with the scaffolds. In the untreated group, the outer surface of the scaffold was still surrounded by obvious osteoid tissues, and the inner surface of the scaffold had less mineralized bone apposition than the MAO-treated group. Apart from that, a more refined quantitative analysis can be followed up.

Conclusions

Different surface modification methods of materials have different effects on osteogenesis. Although MAO treatment may produce a few microcracks, it has obvious advantages (28). MAO was used to construct a multistage pore structure coating on the surface of 3D-printed porous titanium scaffolds. The coating was biologically active because of its Ca/P-rich content. It has been confirmed that the coating on titanium alloy surface constructed by MAO can effectively reduce the release of cytotoxic Al and V elements, and the Ca/P in the coating can be dissolved in a small amount in a calcium-deficient environment which can promote the deposition of hydroxyapatite (29-31). The micro-nano porous structure and chemical composition of the coating enabled better biocompatibility
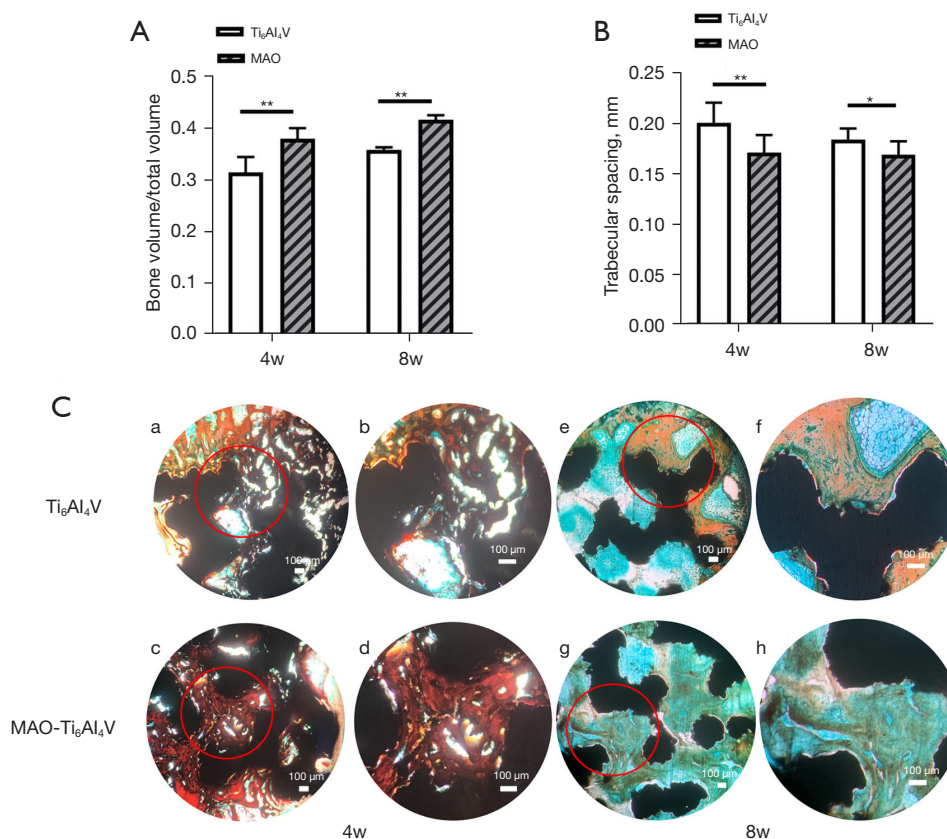
Figure 7 Evaluation of bone ingrowth and osseointegration of scaffolds in *in vitro* experiment in two groups of scaffolds. (A,B) Quantitative results of bone fractions in the peri-scaffold region and intra-porous region of the scaffolds. *, P<0.05; **, P<0.01. Sample number =8 in each group. (C) Light optical micrographs of the histological sections stained with Masson Goldner's trichrome of the untreated and MAO-treated scaffolds at 4 and 8 weeks after surgery. The red circles in (a,c,e,g) correspond to (b,d,f,h), respectively. The mineralized bone tissues are stained in green, the osteoid tissues are stained in red/orange, and the scaffolds appear in black. MAO, micro-arc oxidation.

and osteogenic induction of the porous titanium scaffold. The MAO-treated scaffolds showed good biocompatibility *in vitro* and osseointegration capacity *in vivo*. At present, researches on MAO are no longer limited to enhancing the osteogenic properties of the base material, but also includes antibacterial properties (32,33). In addition to this, MAO is becoming more efficient and environmentally friendly (34).

MAO may provide a facile approach for the fabrication of bioactive 3D-printed porous implants for orthopedic applications. In the future, in addition to further industrial mass production of MAO, the micro-nano porous structure of MAO treatment may be fully utilised in subsequent research to load different bioactive substances or drugs to expand the therapeutic range and efficacy.

Footnote

Reporting Checklist: The authors have completed the ARRIVE reporting checklist. Available at https://atm.amegroups.com/article/view/10.21037/atm-22-2536/rc

Data Sharing Statement: Available at https://atm.amegroups.

Page 10 of 11

Ni et al. MAO modification of porous Ti$_6$Al$_4$V

com/article/view/10.21037/atm-22-2536/dss

Conflicts of Interest: All authors have completed the ICMJE uniform disclosure form (available at https://atm.amegroups. com/article/view/10.21037/atm-22-2536/coif). CW is from Beijing AK Medical Co., Ltd. The other authors have no conflicts of interest to declare.

Ethical Statement: The authors are accountable for all aspects of the work in ensuring that questions related to the accuracy or integrity of any part of the work are appropriately investigated and resolved. Experiments were performed under a project license (No. LA2014214) granted by Experimental Animal Ethics Committee of Peking University, in compliance with national guidelines for the care and use of animals.

References

1. Geetha M, Singh AK, Asokamani R, et al. Ti based biomaterials, the ultimate choice for orthopaedic implants–a review. Prog Mater Sci 2009;54:397-425.
2. Kunii T, Mori Y, Tanaka H, et al. Improved Osseointegration of a TiNbSn Alloy with a Low Young's Modulus Treated with Anodic Oxidation. Sci Rep 2019;9:13985.
3. Chen S, Lee CY, Li RW, et al. Modelling osteoblast adhesion on surface-engineered biomaterials: optimisation of nanophase grain size. Comput Methods Biomech Biomed Engin 2017;20:905-14.
4. Maniar RN, Singhi T. Patient specific implants: scope for the future. Curr Rev Musculoskelet Med 2014;7:125-30.
5. Cheng A, Cohen DJ, Kahn A, et al. Laser Sintered Porous Ti-6-4V Implants Stimulate Vertical Bone Growth. Ann Biomed Eng 2017;45:2025-35.
6. Cheong VS, Fromme P, Coathup MJ, et al. Partial Bone Formation in Additive Manufactured Porous Implants Reduces Predicted Stress and Danger of Fatigue Failure.

7. Ann Biomed Eng 2020;48:502-14.
8. Hollister SJ. Scaffold design and manufacturing: from concept to clinic. Adv Mater 2009;21:3330-42.
9. Bonfield W. Designing porous scaffolds for tissue engineering. Philos Trans A Math Phys Eng Sci 2006;364:227-32.
10. Frosch KH, Barvencik F, Viereck V, et al. Growth behavior, matrix production, and gene expression of human osteoblasts in defined cylindrical titanium channels. J Biomed Mater Res A 2004;68:325-34.
11. Lv J, Xiu P, Tan J, et al. Enhanced angiogenesis and osteogenesis in critical bone defects by the controlled release of BMP-2 and VEGF: implantation of electron beam melting-fabricated porous Ti6Al4V scaffolds incorporating growth factor-doped fibrin glue. Biomed Mater 2015;10:035013.
12. Yavari SA, Wauthlé R, Böttger AJ, et al. Crystal structure and nanotopographical features on the surface of heat-treated and anodized porous titanium biomaterials produced using selective laser melting. Appl Surf Sci 2014;290:287-94.
13. Abar B, Kelly C, Pham A, et al. Effect of surface topography on in vitro osteoblast function and mechanical performance of 3D printed titanium. J Biomed Mater Res A 2021;109:1792-802.
14. Yang J, Cai H, Lv J, et al. In vivo study of a self-stabilizing artificial vertebral body fabricated by electron beam melting. Spine (Phila Pa 1976) 2014;39:E486-92.
15. Pereira Sousa TS, da Costa N de A, Nespeque Correa DR, et al. Morphology, crystalline structure and chemical composition of MAO treated Ti-15Zr-Mo surfaces enriched with bioactive ions. Materials Research 2019;22:e20190005.
16. Kokubun R, Wang W, Zhu S, et al. In vivo evaluation of a Ti-based bulk metallic glass alloy bar. Biomed Mater Eng 2015;26:9-17.
17. Neuhoff D, Thompson RE, Frauchiger VM, et al. Anodic plasma chemical treatment of titanium Schanz screws reduces pin loosening. J Orthop Trauma 2005;19:543-50.
18. Sikdar S, Menezes PV, Maccione R, et al. Plasma Electrolytic Oxidation (PEO) Process-Processing, Properties, and Applications. Nanomaterials (Basel) 2021;11:1375.
19. Guan S, Qi M, Wang C, et al. Enhanced cytocompatibility of Ti6Al4V alloy through selective removal of Al and V from the hierarchical micro-arc oxidation coating. Appl Surf Sci 2021;541:148547.
20. Jian SY, Aktug SL, Huang HT, et al. The Potential of

Calcium/Phosphate Containing MAO Implanted in Bone Tissue Regeneration and Biological Characteristics. Int J Mol Sci 2021;22:4706.

20. Gao H, Jie YF, Wang ZQ, et al. Bioactive tantalum metal prepared by micro-arc oxidation and NaOH treatment. J Mater Chem B 2014;2:1216-24.

21. Li LH, Kong YM, Kim HW, et al. Improved biological performance of Ti implants due to surface modification by micro-arc oxidation. Biomaterials 2004;25:2867-75.

22. Zhou R, Wei D, Cheng S, et al. Structure, MC3T3-E1 cell response, and osseointegration of macroporous titanium implants covered by a bioactive microarc oxidation coating with microporous structure. ACS Appl Mater Interfaces 2014;6:4797-811.

23. Wu J, Liu R, Wang B, et al. Preparation and characterization of carburized layer on pure aluminum by plasma electrolysis. Surf Coat Technol 2015;269:119-24.

24. Fan X, Feng B, Di Y, et al. Preparation of bioactive TiO film on porous titanium by micro-arc oxidation. Appl Surf Sci 2012;258:7584-8.

25. Jing Z, Ni R, Wang J, et al. Practical strategy to construct anti-osteosarcoma bone substitutes by loading cisplatin into 3D-printed titanium alloy implants using a thermosensitive hydrogel. Bioact Mater 2021;6:4542-57.

26. Wang X, Yu Y, Ji L, et al. Calcium phosphate-based materials regulate osteoclast-mediated osseointegration. Bioact Mater 2021;6:4517-30.

27. Tsai MT, Chang YY, Huang HL, et al. Micro-arc oxidation treatment enhanced the biological performance of human osteosarcoma cell line and human skin fibroblasts cultured on titanium–zirconium films. Surf Coat Technol 2016;303:268-76.

28. Liu J, Mohd Rafiq NB, Wong LM, et al. Surface Treatment and Bioinspired Coating for 3D-Printed Implants. Front Chem 2021;9:768007.

29. Li Y, Wang W, Yu F, et al. Characterization and cytocompatibility of hierarchical porous TiO2 coatings incorporated with calcium and strontium by one-step micro-arc oxidation. Mater Sci Eng C Mater Biol Appl 2020;109:110610.

30. Fialho L, Grenho L, Fernandes MH, et al. Porous tantalum oxide with osteoconductive elements and antibacterial core-shell nanoparticles: A new generation of materials for dental implants. Mater Sci Eng C Mater Biol Appl 2021;120:111761.

31. Santos-Coquillat A, Tenorio RG, Mohedano M, et al. Tailoring of antibacterial and osteogenic properties of Ti6Al4V by plasma electrolytic oxidation. Appl Surf Sci 2018;454:157-72.

32. Li B, Yang T, Sun R, et al. Biological and antibacterial properties of composite coatings on titanium surfaces modified by microarc oxidation and sol-gel processing. Dent Mater J 2021;40:455-63.

33. Warsi MF, Chaudhary K, Zulfiqar S, et al. Copper and silver substituted MnO2 nanostructures with superior photocatalytic and antimicrobial activity. Ceram Int 2022;48:4930-9.

34. Zaniolo KM, Biaggio SR, Cirelli JA, et al. Physical characterization and biological tests of bioactive titanium surfaces prepared by short-time micro-arc oxidation in green electrolyte. Mater Res Express 2022;9:025401.